

Theoretical analysis on the possibility of superconductivity in a trilayer Ruddlesden-Popper nickelate $\text{La}_4\text{Ni}_3\text{O}_{10}$ under pressure and its experimental examination : comparison with $\text{La}_3\text{Ni}_2\text{O}_7$

Hirofumi Sakakibara,^{1,*} Masayuki Ochi,^{2,3,*} Hibiki Nagata,^{4,5,*} Yuta Ueki,^{4,5,*}
Hiroya Sakurai,^{4,*} Ryo Matsumoto,⁴ Kensei Terashima,⁴ Keisuke Hirose,⁶
Hiroto Ohta,⁶ Masaki Kato,⁶ Yoshihiko Takano,^{4,5,†} and Kazuhiko Kuroki^{2,‡}

¹*Advanced Mechanical and Electronic System Research Center(AMES), Faculty of Engineering, Tottori University, 4-10 Koyama-cho, Tottori, Tottori 680-8552, Japan*

²*Department of Physics, Osaka University, 1-1 Machikaneyama-cho, Toyonaka, Osaka 560-0043, Japan*

³*Forefront Research Center, Osaka University, 1-1 Machikaneyama-cho, Toyonaka, Osaka 560-0043, Japan*

⁴*MANA, National Institute for Materials Science (NIMS), 1-2-1 Sengen, Tsukuba 305-0047 Japan*

⁵*University of Tsukuba, 1-1-1 Tennodai, Tsukuba, Ibaraki 305-8577, Japan*

⁶*Department of Molecular Chemistry and Biochemistry, Doshisha University, 1-3 Tataramiyakotani, Kyo-Tanabe 610-0321, Japan*

(Dated: December 3, 2024)

We study the possibility of superconductivity in a trilayer Ruddlesden-Popper nickelate $\text{La}_4\text{Ni}_3\text{O}_{10}$ under pressure both theoretically and experimentally, making comparison with the recently discovered high T_c superconductor $\text{La}_3\text{Ni}_2\text{O}_7$, a bilayer nickelate. Through DFT calculations, we find that a structural phase transition from monoclinic to tetragonal takes place around 20–40 GPa. Using the crystal structure obtained at 40 GPa, we theoretically investigate the possibility of superconductivity, where a combination of fluctuation exchange approximation and linearized Eliashberg equation is applied to a six-orbital model constructed from first principles band calculation. The obtained results suggests that $\text{La}_4\text{Ni}_3\text{O}_{10}$ may also become superconducting under high pressure with T_c comparable to some cuprates, although it is not as high as $\text{La}_3\text{Ni}_2\text{O}_7$. We also perform experimental studies using our polycrystalline samples of $\text{La}_3\text{Ni}_2\text{O}_{7.12}$ and $\text{La}_4\text{Ni}_3\text{O}_{9.99}$. The superconducting transition of $\text{La}_3\text{Ni}_2\text{O}_{7.12}$, with a maximum onset T_c of 78.4 K at a pressure of 26.1 GPa, is confirmed by a drop in the electrical resistance, as well as the magnetic field dependence of the resistance. Quite interestingly, similar temperature and magnetic field dependences of the resistance are observed also for $\text{La}_4\text{Ni}_3\text{O}_{9.99}$, where a drop in the resistance is observed at lower temperatures compared to $\text{La}_3\text{Ni}_2\text{O}_{7.12}$, under pressures of 32.8 GPa and above. Given the theoretical expectation, the reduction in the resistance can most likely be attributed to the occurrence of superconductivity in $\text{La}_4\text{Ni}_3\text{O}_{9.99}$.

I. INTRODUCTION

Even vs. odd number effects have often been issues of interest in various fields of physics. A famous example in condensed matter physics is the Haldane’s conjecture, which states that in a spin- $N/2$ antiferromagnetic Heisenberg chain, the excitation spectrum is gapless and the spin-spin correlation exhibits a slow (algebraic) decay when N is an odd number, whereas when N is even, there is a gap in the excitation and the spin correlation decays exponentially [1]. Schulz discussed the relation between spin- $N/2$ antiferromagnetic Heisenberg chain and N coupled spin-1/2 chains [2, 3], namely, N -leg ladders, and argued that when N is even, the system is gapful, while the system becomes gapless when N is odd. In the 1990’s, following the studies by Dagotto *et al.*[4] and by Rice *et al.*[5], spin-1/2 antiferromagnetic N -leg ladders were intensively studied both theoretically and experimentally [6]. Due to the opening of the spin gap in the

case of $N = \text{even}$, the possibility of superconductivity in doped even-leg (two-leg in particular) Hubbard and t - J models was widely investigated both analytically and numerically [4–6]. Indeed, a cuprate that contains two-leg ladders was found to superconduct under pressure [7].

Here, an interesting problem arises regarding the possibility of superconductivity in doped *odd*-number-leg ladders. One might expect absence of superconductivity due to the absence of the spin gap, but one of the present authors and his colleagues showed that superconductivity can still take place in the three-leg Hubbard ladder [8], based on the weak coupling analysis that shows two out of three spin modes are gapped [9, 10]. A similar result was also obtained in Ref. [3], and the weak coupling analysis was soon extended to N -leg ladders [11].

A two dimensional analogue of the two-leg ladder model, namely, the bilayer model, typically on a square lattice, has also been a target of theoretical interest from the perspective of unconventional superconductivity. When two square lattices are coupled by a large vertical hopping t_\perp or a strong vertical magnetic coupling J_\perp , opening of a spin gap is expected, and various studies have shown strong enhancement of interlayer pairing superconductivity [4, 12–20]. Motivated by the

* These five authors contributed equally

† TAKANO.Yoshihiko@nims.go.jp

‡ kuroki@presto.phys.sci.osaka-u.ac.jp

very strong enhancement of superconductivity near half filling found in some studies [13, 14], one of the present authors investigated the possibility of realizing the bilayer Hubbard model with large t_{\perp} in actual materials, and ended up with a bilayer Ruddlesden-Popper nickelate $\text{La}_3\text{Ni}_2\text{O}_7$ [16]. The key factor there was that the Ni $3d_{3z^2-r^2}$ orbitals, which are elongated in the out-of-plane direction and hence enhance t_{\perp} , are close to half filling in this material. Quite recently, superconductivity in the very $\text{La}_3\text{Ni}_2\text{O}_7$ with a maximum T_c of 80K has been discovered under high pressure [21], which has sparked a vast wave of interest both experimentally [22–24] and theoretically [25–51] including ours [52].

Given the recent developments in the bilayer $\text{La}_3\text{Ni}_2\text{O}_7$, and also the previous studies regarding even vs. odd-leg ladders as described above, it is natural to consider investigating the possibility of superconductivity in a trilayer Ruddlesden-Popper nickelate $\text{La}_4\text{Ni}_3\text{O}_{10}$. Since $\text{La}_4\text{Ni}_3\text{O}_{10}$ is not superconducting at ambient pressure, we will consider its possibility under pressure as in $\text{La}_3\text{Ni}_2\text{O}_7$ both theoretically and experimentally. Since superconductivity in $\text{La}_3\text{Ni}_2\text{O}_7$ appears to occur when the symmetry of the crystal structure becomes (close to) tetragonal under high pressure [21], we first investigate theoretically whether the crystallographic symmetry of $\text{La}_4\text{Ni}_3\text{O}_{10}$ becomes tetragonal under high pressure. Indeed, we find that a structural phase transition from monoclinic to tetragonal takes place around 20–40 GPa. Adopting a hypothesis that superconductivity in $\text{La}_4\text{Ni}_3\text{O}_{10}$, if any, occurs when the crystallographic symmetry is tetragonal, we investigate the possibility of superconductivity using the crystal structure obtained at 40 GPa, where a combination of fluctuation exchange approximation (FLEX) and linearized Eliashberg equation is applied to a six-orbital (2 orbitals \times 3 layers) model constructed from first principles band calculation. Our calculation results suggest that $\text{La}_4\text{Ni}_3\text{O}_{10}$ may also become superconducting under high pressure with T_c comparable to some cuprates, although it is not as high as $\text{La}_3\text{Ni}_2\text{O}_7$.

We also present experimental results for our polycrystalline samples of $\text{La}_3\text{Ni}_2\text{O}_{7.12}$ and $\text{La}_4\text{Ni}_3\text{O}_{9.99}$. The superconducting transition of $\text{La}_3\text{Ni}_2\text{O}_{7.12}$, with a maximum onset T_c of 78.4 K at a pressure of 26.1 GPa, is confirmed by a drop in the electrical resistance, as well as the magnetic field dependence of the resistance. Quite interestingly, similar temperature and magnetic field dependences of the resistance are observed also for $\text{La}_4\text{Ni}_3\text{O}_{9.99}$, where a drop in the resistance is observed at lower temperatures compared to $\text{La}_3\text{Ni}_2\text{O}_{7.12}$, under pressures of 32.8 GPa and above. Given the theoretical expectation, the reduction in the resistance can most likely be attributed to the occurrence of superconductivity in $\text{La}_4\text{Ni}_3\text{O}_{9.99}$.

II. THEORETICAL METHOD

For density functional theory (DFT) calculation, we use the PBEsol exchange-correlation functional [53] and the projector augmented wave method [54] as implemented in *Vienna ab initio Simulation Package* (VASP) [55–58]. Core-electron states in PAW potentials are $[\text{Kr}]4d^{10}$, $[\text{Ar}]$, $[\text{He}]$ for La, Ni, O, respectively. We use a plane-wave cutoff energy of 600 eV for Kohn-Sham orbitals without including the spin-orbit coupling for simplicity.

We perform structural optimization until the Hellmann-Feynman force becomes less than 0.01 eV \AA^{-1} for each atom using an $8 \times 8 \times 2$ \mathbf{k} -mesh. To verify the stability of the optimized crystal structure under pressure, we calculate the phonon dispersion using the finite displacement method as implemented in the PHONOPY [59] software in combination with VASP. We use a $4 \times 4 \times 1$ \mathbf{q} -mesh for a conventional tetragonal unit cell containing 34 atoms. For a $4 \times 4 \times 1$ supercell used for finite-displacement calculations, we use a $3 \times 3 \times 2$ \mathbf{k} -mesh.

To discuss superconductivity, we extract Ni- $d_{x^2-y^2}$ and $d_{3z^2-r^2}$ Wannier orbitals using WANNIER90 software [60–62]. For this purpose, we use the tetragonal crystal structure under pressure of 40 GPa obtained by our calculation. We use an $12 \times 12 \times 12$ \mathbf{k} -mesh for a primitive unit cell. We study the possibility of superconductivity for the obtained six-orbital model within FLEX [63, 64]. As for the interaction term of the Hamiltonian, we take the on-site interactions, namely, intraorbital(interorbital) Coulomb interactions $U(U')$, Hund’s coupling J , and pair hopping J' . We assume the orbital rotational symmetry, and take the same value of U for the $d_{x^2-y^2}$ and the $d_{3z^2-r^2}$ orbitals, and $U' = U - 2J$, $J = J'$. As a typical value of the interactions, we take $U = 3$ eV, $J = J' = 0.3$ eV and $U' = U - 2J = 2.4$ eV. We calculate the self-energy induced by the spin-fluctuation formulated as shown in the literatures [65–67] in a self-consistent calculation. The real part of the self-energy at the lowest Matsubara frequency is subtracted in the same manner with Ref. [68] to maintain the band structure around the Fermi level obtained by first-principles calculation.

The obtained Green’s function and the pairing interaction, mediated mainly by spin fluctuations, are plugged into the linearized Eliashberg equation. Since the the eigenvalue λ of the Eliashberg equation monotonically increases upon lowering the temperature, and reaches unity at $T = T_c$, we adopt λ calculated at a fixed temperature, $T = 0.01$ eV as a measure of superconductivity. For convenience, we will call the eigenfunction (with the largest eigenvalue) of the linearized Eliashberg equation at the lowest Matsubara frequency $i\omega(=i\pi k_B T)$ the “superconducting gap function”. We take a $16 \times 16 \times 4$ k -point mesh and 2048 Matsubara frequencies for the FLEX calculation.

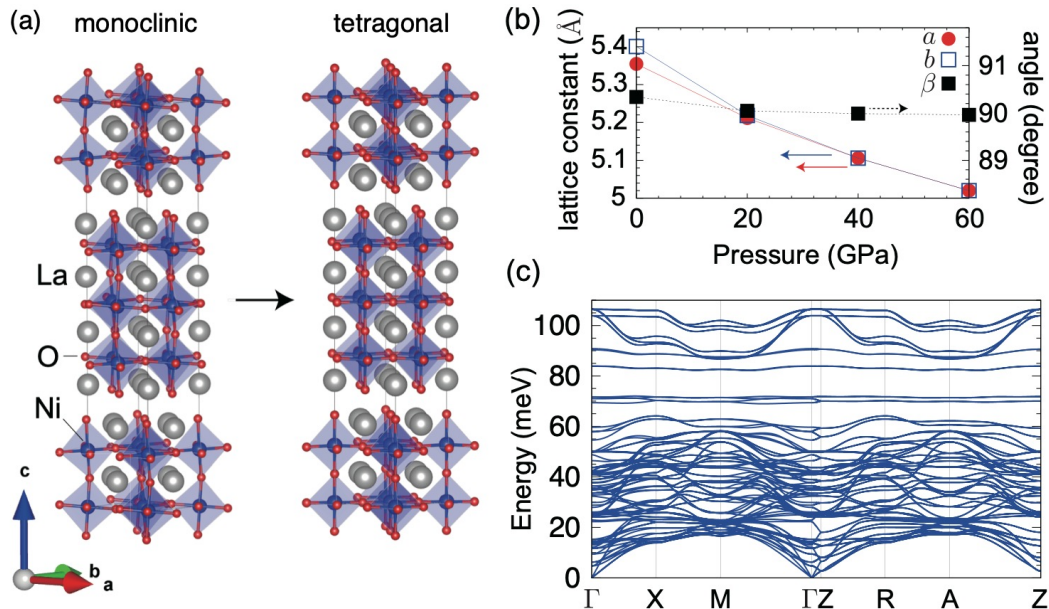


FIG. 1. (a) Optimized crystal structures of $\text{La}_4\text{Ni}_3\text{O}_{10}$ under pressure of 0 GPa (monoclinic) and 40 GPa (tetragonal). Gray, blue, and red spheres denote La, Ni, and O atoms, respectively. Crystal structure was depicted using the VESTA software [69]. (b) Lattice parameters a , b , and β obtained by structural optimization with the $P2_1/a$ ($Z = 4$) space group under pressure. (c) Phonon dispersion of the tetragonal $I4/mmm$ structure under pressure of 40 GPa.

III. EXPERIMENTAL METHOD

Polycrystalline samples of $\text{La}_3\text{Ni}_2\text{O}_{7.12}$ and $\text{La}_4\text{Ni}_3\text{O}_{9.99}$ were employed for electrical resistance measurements under high-pressure conditions. These were synthesized from La_2O_3 and NiO , and characterized by powder X-ray diffraction and thermogravimetry to find that they were of single phases with the chemical compositions. The details of the synthesis and characterization will be described elsewhere [70]. High pressure was generated with Diamond Anvil Cell (DAC) with boron-doped diamond electrodes designed for four-terminal resistance measurement [71, 72]. Cubic boron nitride powder was used as a pressure-transmitting medium. Applied pressure was estimated by fluorescence of ruby placed near the sample up to 20 GPa [73]. For pressure beyond 20 GPa, applied pressure was estimated by a Raman spectrum from a culet of the top diamond anvil obtained by Raman Microscope (Renishaw)[74]. Details of the cell configuration will be described in the literatures [75, 76]. Temperature and magnetic fields were controlled by PPMS (Quantum Design).

IV. THEORETICAL RESULTS—CRYSTAL STRUCTURE

We optimized the crystal structure under pressure by DFT calculation. Here, we note that several different space groups have been reported in literature for $\text{La}_4\text{Ni}_3\text{O}_{10}$ at ambient pressure, $Fmmm$ [77] (or $Imm2$ considering a symmetry lowering mentioned in this study, as pointed out in Ref. 78), $Cmce$ ($Bmab$) [78–80], $P2_1/a$ ($Z = 4$) (i.e., $P2_1/a$ containing 4 formula units in the unit cell) [81–83] as was also reported for $\text{Nd}_4\text{Ni}_3\text{O}_{10-\delta}$ [84, 85], and $P2_1/a$ ($Z = 2$) [78, 86] as was also reported for $\text{Pr}_4\text{Ni}_3\text{O}_{10}$ [87]. It was pointed out that samples were mixed phases of orthorhombic and monoclinic symmetry [78, 88]. The stability of several phases, $Cmce$, $Pbca$, and two types of $P2_1/a$, was also investigated by DFT calculation [89]. Due to the complexity of the situation, we first optimized a crystal structure under pressure assuming a monoclinic space group of $P2_1/a$ ($Z = 4$), which has a relatively low symmetry among these candidates and is a subgroup of some of the candidates, and next checked the stability of the obtained structure under pressure by phonon calculation.

By the structural optimization of an $P2_1/a$ ($Z = 4$) structure under pressure, we found that the structural phase transition from monoclinic to tetragonal takes place as shown in Fig. 1(a). In fact, lattice parameters relevant to the monoclinic-tetragonal transition, a , b , and β , were shown in Fig. 1(b), where $a = b$ and $\beta = 90^\circ$ were realized at around 20–40 GPa. We also confirmed that the obtained tetragonal structure belongs to the $I4/mmm$ space group by checking atomic coordinates. Then, we performed phonon calculation for the tetragonal $I4/mmm$ structure under pressure of 40 GPa. The calculated phonon dispersion has no imaginary modes as shown in Fig. 1(c), by which we confirmed the stability of this structure. Our calculation shows that several tens of gigapascal pressure gives rise to a tetragonal structure, as in $\text{La}_3\text{Ni}_2\text{O}_7$ [21].

V. THEORETICAL RESULTS—BAND STRUCTURE AND SUPERCONDUCTIVITY

We now study the possibility of superconductivity in the tetragonal phase, which can be considered as natural due to the enhanced electronic hopping between the layers, which is likely to favor interlayer pairing superconductivity, as in $\text{La}_3\text{Ni}_2\text{O}_7$. In Fig. 2(b), we present the band structure of the six-orbital model of $\text{La}_4\text{Ni}_3\text{O}_{10}$ at 40 GPa. Some of the key parameter values are listed in table I. For comparison, in Fig. 2(a), we also show the band structure of the four-orbital model of $\text{La}_3\text{Ni}_2\text{O}_7$ obtained in our previous study [52]. While there are bonding (colored blue) and anti-bonding (green) $d_{3z^2-r^2}$ bands in $\text{La}_3\text{Ni}_2\text{O}_7$, in $\text{La}_4\text{Ni}_3\text{O}_{10}$, there is an additional non-bonding $d_{3z^2-r^2}$ band (yellow) between the bonding and anti-bonding bands. Interestingly, the Fermi level in $\text{La}_4\text{Ni}_3\text{O}_{10}$ is placed near the top of the bonding $d_{3z^2-r^2}$ band, while the bottom of the anti-bonding band is placed somewhat above the Fermi level, which is a situation similar to that in $\text{La}_3\text{Ni}_2\text{O}_7$. This similarity occurs due to a combination of two discrepancies between these materials, namely, (i) there is a non-bonding $d_{3z^2-r^2}$ band in $\text{La}_4\text{Ni}_3\text{O}_{10}$, and (ii) the formal Ni valence is +2.67 in $\text{La}_4\text{Ni}_3\text{O}_{10}$ against +2.5 in $\text{La}_3\text{Ni}_2\text{O}_7$.

TABLE I. The orbital level offset $\Delta E = E_{x^2-y^2} - E_{3z^2-r^2}$ between $d_{x^2-y^2}$ and $d_{3z^2-r^2}$ orbitals, the vertical interlayer hopping t_\perp between the $d_{3z^2-r^2}$ orbitals, the nearest-neighbor intralayer hoppings $t_{3z^2-r^2}$, $t_{x^2-y^2}$, and $t_{x^2-y^2-3z^2-r^2}$ of $\text{La}_4\text{Ni}_3\text{O}_{10}$ are displayed. Here, the onsite energy offset between the inner- and outer-layer $d_{x^2-y^2}$ ($d_{3z^2-r^2}$) orbitals is 0.262 eV (0.415 eV). The first column indicates the layer difference of parameters. The parameters of $\text{La}_3\text{Ni}_2\text{O}_7$ presented in Ref. [52] are also displayed in the lowest row for comparison.

[eV]	ΔE	t_\perp	$t_{3z^2-r^2}$	$t_{x^2-y^2}$	$t_{x^2-y^2-3z^2-r^2}$
inner	0.105		-0.163	-0.541	-0.294
outer	0.257	-0.712	-0.117	-0.538	-0.285
$\text{La}_3\text{Ni}_2\text{O}_7$	0.372	-0.664	-0.117	-0.491	-0.242

Let us now see how this similarity and discrepancies of the band structure between the two materials is reflected in superconductivity. In Fig. 2(c), the eigenvalue of the Eliashberg equation λ of the six-orbital model of $\text{La}_4\text{Ni}_3\text{O}_{10}$ is plotted against the band filling (defined as the number of electrons per unit cell per spin), which is measured from that of the stoichiometric composition (two electrons). For comparison, we plot λ for the four-orbital model of $\text{La}_3\text{Ni}_2\text{O}_7$ [52]. The eigenvalue is found to be smaller for $\text{La}_4\text{Ni}_3\text{O}_{10}$ than for $\text{La}_3\text{Ni}_2\text{O}_7$, but a notable difference regarding the band filling dependence is that while λ monotonically decreases for $\text{La}_3\text{Ni}_2\text{O}_7$ when the band filling is decreased, namely, when it moves away from half filling, for $\text{La}_4\text{Ni}_3\text{O}_{10}$, λ is (locally) maximized near the stoichiometric composition. Consequently, its value (0.433) for $\text{La}_4\text{Ni}_3\text{O}_{10}$ at stoichiometry is not small, in the sense that it is still comparable to those of some of the cuprates (with relatively low T_c) obtained by the same method [90–92]. The relatively small reduction of λ compared to that of $\text{La}_3\text{Ni}_2\text{O}_7$ is even more interesting considering the fact that the band filling of the $d_{3z^2-r^2}$ orbitals in $\text{La}_4\text{Ni}_3\text{O}_{10}$ is only roughly 1/3 (per Ni atom per spin), compared to roughly 1/2 (half filling) in $\text{La}_3\text{Ni}_2\text{O}_7$, so that the electron correlation effects are expected to be significantly smaller in the former.

In order to understand the origin of the band filling dependence of λ , we plot in Fig. 2(e) the superconducting gap function of the model of $\text{La}_4\text{Ni}_3\text{O}_{10}$ for various band fillings, together with that of $\text{La}_3\text{Ni}_2\text{O}_7$ (at stoichiometry) obtained in Ref. [52] (Fig. 2(d)). At stoichiometry in $\text{La}_4\text{Ni}_3\text{O}_{10}$, the sign of the gap is reversed not only between bonding and anti-bonding $d_{3z^2-r^2}$ bands (as in $\text{La}_3\text{Ni}_2\text{O}_7$), but also between bonding and non-bonding bands. When the band filling is decreased from stoichiometry (when holes are doped), the superconducting gap of the anti-bonding band becomes small, while when electrons are doped, the gap of the non-bonding band becomes small. Also, all the bands are fully gapped at stoichiometry, while the small gaps are nodal when doped. From these results, we may conclude that the (locally) maximized and relatively large λ obtained for $\text{La}_4\text{Ni}_3\text{O}_{10}$ around stoichiometry, despite $d_{3z^2-r^2}$ orbitals being away from half filling, is because all three $d_{3z^2-r^2}$ bands contribute to superconductivity. This in turn can be attributed to the relation between the Fermi level and the band edges; around stoichiometry, the edge of all three bands touches or lies close to the Fermi level, namely all the bands are (nearly) “incipient”, which pushes up the spin fluctuations to finite energies, thereby making them more effective as pairing glue [16, 93]. When holes are doped, the Fermi level moves away from the anti-bonding band bottom, whereas for electron doping, the Fermi level firmly intersects the non-bonding band. These situations are schematically presented in Fig. 2(f).

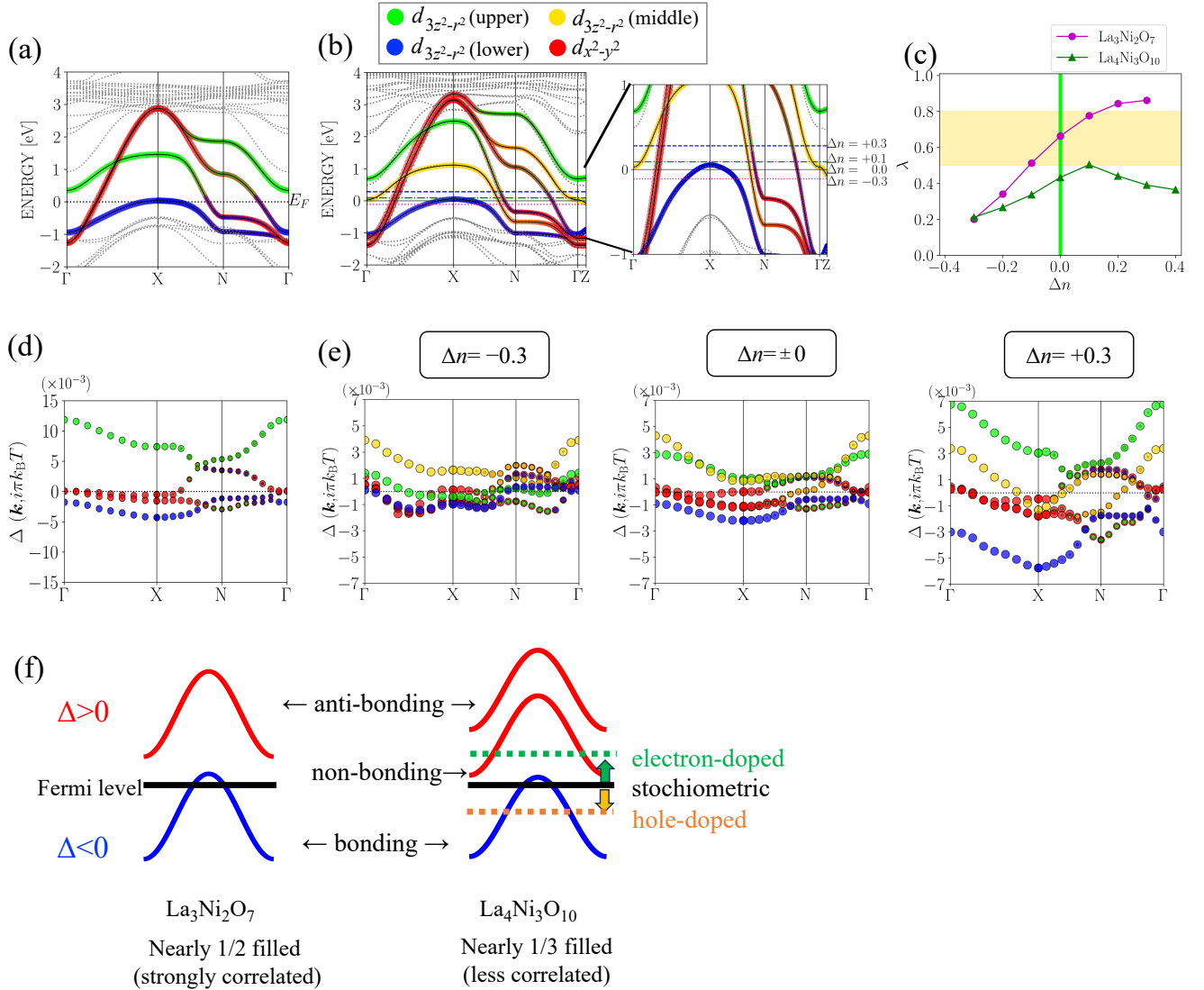


FIG. 2. (a) The band structure of the four-orbital model of $\text{La}_3\text{Ni}_2\text{O}_7$ [52]. (b) The band structure of the six-orbital model of $\text{La}_4\text{Ni}_3\text{O}_{10}$. On the right is a blowup near the Fermi level, together with the Fermi level for various band fillings. (c) The eigenvalue of the Eliashberg equation for $\text{La}_4\text{Ni}_3\text{O}_{10}$ and $\text{La}_3\text{Ni}_2\text{O}_7$ [52] plotted against the band filling measured from stoichiometry. The yellow hatched region indicates the range of λ obtained by the same method for various cuprates [90–92]. (d) Superconducting gap functions of $\text{La}_3\text{Ni}_2\text{O}_7$ for $\Delta n = 0$ [52]. (e) Superconducting gap functions of $\text{La}_4\text{Ni}_3\text{O}_{10}$ for $\Delta n = -0.3$ (left), $\Delta n = 0$ (center), $\Delta n = +0.3$ (right). (f) Schematic picture of the superconducting gap functions of $\text{La}_3\text{Ni}_2\text{O}_7$ and $\text{La}_4\text{Ni}_3\text{O}_{10}$. The strength of Wannier orbital characters are presented in panels (a)(b)(d)(e) with the thickness/radius of the color coded line/circles, where the “sum” of the $d_{x^2-y^2}$ ($d_{3z^2-r^2}$) orbital characters among inner- and outer-layer is indicated by red (green, blue, and yellow). The yellow color is used for indicating the $d_{3z^2-r^2}$ characters in the case that the eigenstate contains the inner-layer components less than 5%. Otherwise, either green or blue is used for the $d_{3z^2-r^2}$ components, depending on whether the band energy is above or below 0.2 eV. In this way, the colors blue, yellow, and green represent bonding, non-bonding, and anti-bonding $d_{3z^2-r^2}$ bands, respectively. All the calculation results for $\text{La}_4\text{Ni}_3\text{O}_{10}$ are obtained using the crystal structure at 40 GPa.

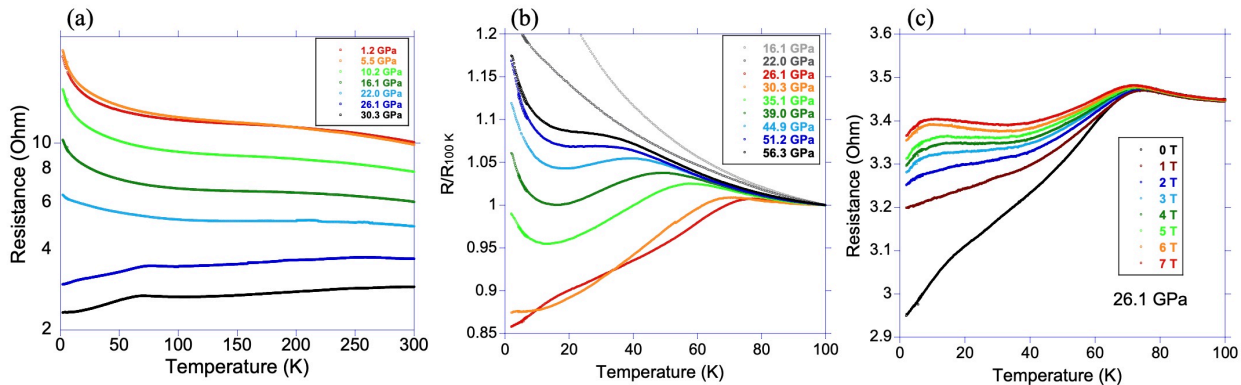


FIG. 3. Temperature dependence of the electrical resistance of $\text{La}_3\text{Ni}_2\text{O}_{7.12}$ (a) under several pressures from 1.2 to 30.3 GPa, (b) normalized at 100 K, under 16.1 - 56.3 GPa, (c) under magnetic fields from 0 to 7 T, at 26.1 GPa.

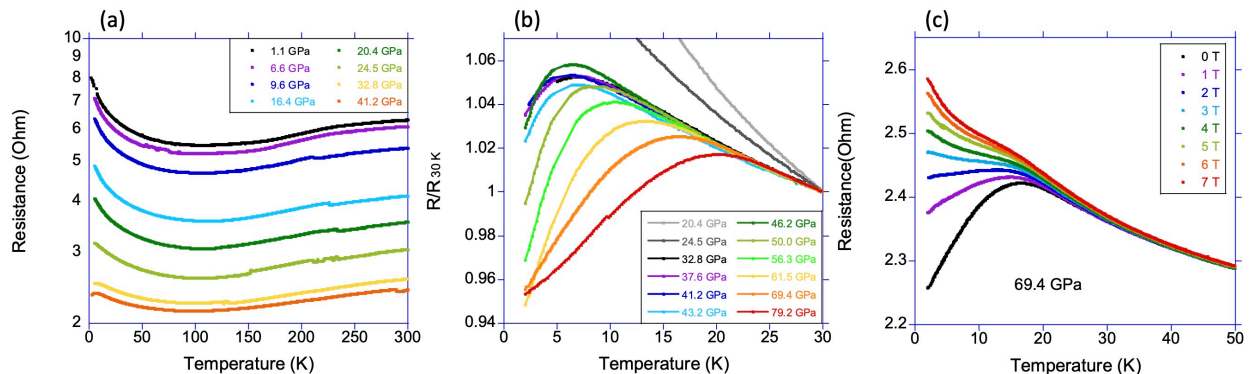


FIG. 4. Temperature dependence of the electrical resistance of $\text{La}_4\text{Ni}_3\text{O}_{9.99}$ (a) under several pressures from 1.1 to 41.2 GPa, (b) normalized at 30 K, under several pressures from 32.8 to 79.2 GPa, (c) under magnetic fields from 0 to 7 T, at 69.4 GPa.

VI. EXPERIMENTAL RESULTS— $\text{La}_3\text{Ni}_2\text{O}_{7.12}$

We now turn to the experimental results. We first focus on $\text{La}_3\text{Ni}_2\text{O}_{7.12}$. Fig. 3 displays the temperature dependence of the electrical resistance under various pressures and magnetic fields. Semiconducting behavior is observed below 22.0 GPa, whereas metallic behavior emerges at 26.1 and 30.3 GPa, as shown in Fig. 3(a). At 26.1 GPa, the superconducting transition with an onset T_c around 78.4 K is clearly recognized, which is a behavior similar to that of $\text{La}_3\text{Ni}_2\text{O}_7$ single crystals in the previous studies [21, 23, 24], although the amount of the resistance drop is not as significant as in those studies. T_c

appears to decrease with increasing pressure as shown in Fig. 3(b). The superconductivity survives even at magnetic fields of 7 T, although the resistance drop below T_c diminishes significantly with increasing field, as shown in Fig. 3(c). T_c exhibits small field dependence, i.e., 78.4 K (0 T) to 74.1 K (7 T), which is also consistent with the previous studies [21, 23, 24].

VII. EXPERIMENTAL RESULTS— $\text{La}_4\text{Ni}_3\text{O}_{9.99}$

We now present experimental results for $\text{La}_4\text{Ni}_3\text{O}_{9.99}$. Fig. 4 shows the temperature dependence of the electrical

resistance under various pressures and magnetic fields. $\text{La}_4\text{Ni}_3\text{O}_{9.99}$ displays metallic behavior across all measured pressures, with a slight upturn observed at temperatures below approximately 100 K, as shown in Fig. 4(a). The origin of the upturn is uncertain at present. Intriguingly, the drop in resistance suddenly appears below 5 K at 32.8 GPa. Upon increasing the pressure beyond 46.2 GPa, the temperature at which the resistance is maximized increases, and also the decrease in the resistance below it becomes more pronounced, as seen in Fig. 4(b). Here, it should be reminded that according to our theoretical calculation, the tetragonal structure is stabilized beyond pressures around 20–40 GPa in $\text{La}_4\text{Ni}_3\text{O}_{10}$, for which superconductivity with a T_c lower than that of $\text{La}_3\text{Ni}_2\text{O}_7$ is expected to take place around stoichiometric composition. Therefore, the reduction in the resistance can most likely be attributed to pressure induced superconductivity of $\text{La}_4\text{Ni}_3\text{O}_{9.99}$, although the magnitude of the resistance drop is not as significant as in single crystal $\text{La}_3\text{Ni}_2\text{O}_7$ [21, 23, 24], similarly to our data for polycrystalline $\text{La}_3\text{Ni}_2\text{O}_{7.12}$. In fact, the magnetic field dependence of the resistance is quite similar to that of $\text{La}_3\text{Ni}_2\text{O}_{7.12}$ as shown in 4(c), namely, the peak position of the resistance is nearly unaffected, while the resistance drop becomes less significant with increasing field. On the other hand, as seen in Fig. 4(b), the temperature at which the resistance deviates from a linear behavior, considered as the onset T_c , monotonically increases up to 23 K upon increasing the pressure up to 79.2 GPa, which is a pressure dependence opposite to what is observed in $\text{La}_3\text{Ni}_2\text{O}_{7.12}$ and hence is characteristic of $\text{La}_4\text{Ni}_3\text{O}_{9.99}$.

VIII. CONCLUSION

In the present study, we have investigated the possibility of superconductivity in $\text{La}_4\text{Ni}_3\text{O}_{10}$ under pressure both theoretically and experimentally. Through DFT calculations, we have found that a structural phase transition from monoclinic to tetragonal takes place around 20–40 GPa. Using the crystal structure obtained at 40 GPa, we have theoretically investigated the possibility of superconductivity, where a combination of FLEX and linearized Eliashberg equation is applied to a six-orbital model constructed from first principles band calculation. An interesting feature found here is that the eigenvalue of the Eliashberg equation is (locally) maximized around stoichiometry, reflecting the fact that all of

the three $d_{3z^2-r^2}$ bands contribute to superconductivity around this band filling. Hence our calculation results suggest that $\text{La}_4\text{Ni}_3\text{O}_{10}$, around stoichiometric composition, may become superconducting under high pressure with T_c comparable to some cuprates, although it is not as high as $\text{La}_3\text{Ni}_2\text{O}_7$.

We have also performed experimental studies using our polycrystalline samples of $\text{La}_3\text{Ni}_2\text{O}_{7.12}$ and $\text{La}_4\text{Ni}_3\text{O}_{9.99}$. The superconducting transition of $\text{La}_3\text{Ni}_2\text{O}_{7.12}$ has been confirmed by a drop in the electrical resistance, as well as the magnetic field dependence of the resistance. We have observed a maximum onset T_c of 78.4 K at a pressure of 26.1 GPa. Similar temperature and magnetic field dependences of the resistance have been observed also for $\text{La}_4\text{Ni}_3\text{O}_{9.99}$ under high pressure, where a drop in the resistance is observed at lower temperatures compared to $\text{La}_3\text{Ni}_2\text{O}_{7.12}$. Given the theoretical expectation, the reduction in the resistance can most likely be attributed to the occurrence of superconductivity in $\text{La}_4\text{Ni}_3\text{O}_{9.99}$, although we believe that further studies are necessary for a complete confirmation. The temperature at which the resistance deviates from a linear behavior increases with pressure, which is the opposite of what is observed for $\text{La}_3\text{Ni}_2\text{O}_{7.12}$. Understanding the origin of this difference between the two materials serves as an interesting future study.

During the finalization process of the present study, we came to notice a recent experimental study on polycrystalline samples[94]. The temperature and magnetic field dependences of the resistance in $\text{La}_3\text{Ni}_2\text{O}_7$ observed there are quite similar to our results on $\text{La}_3\text{Ni}_2\text{O}_{7.12}$, while superconductivity is not observed in $\text{La}_4\text{Ni}_3\text{O}_{10}$ under the pressure of up to 50 GPa.

ACKNOWLEDGMENTS

We are supported by JSPS KAKENHI Grant No. JP22K03512 (H. Sakakibara), JP22K04907 (K. K.), JP20H05644 (Y. T.), and JSPS Bilateral Program JPJSBP120214602 (Y. T.). The computing resource is supported by the supercomputer system HOKUSAI in RIKEN, and the supercomputer system (system-B) in the Institute for Solid State Physics, the University of Tokyo.

H.S.(H. Sakakibara) , M.O., H.N., Y.U., and H.S.(H. Sakurai) contributed equally to this work.

-
- [1] F. D. M. Haldane, Phys. Rev. Lett. **50**, 1153 (1983).
 [2] H. Schulz, Phys. Rev. B **34**, 6372 (1986).
 [3] H. Schulz, *Correlated Fermions and Transport in Mesoscopic Systems: Proceedings of the XXXIst Rencontres de Moriond*, Vol. 90 (Atlantica Séguier Frontières, 1996).
 [4] E. Dagotto, J. Riera, and D. Scalapino, Phys. Rev. B **45**,

- 5744 (1992).
 [5] T. M. Rice, S. Gopalan, and M. Sigrist, Europhysics Letters **23**, 445 (1993).
 [6] For a review, E. Dagotto and T.M. Rice, Science **271**, 618 (1996), and references therein.
 [7] M. Uehara, T. Nagata, J. Akimitsu, H. Takahashi,

- N. Mōri, and K. Kinoshita, *J. Phys. Soc. Jpn.* **65**, 2764 (1996).
- [8] T. Kimura, K. Kuroki, and H. Aoki, *Phys. Rev. B* **54**, R9608 (1996).
- [9] E. Arrigoni, *Phys. Lett. A* **215**, 91 (1996).
- [10] E. Arrigoni, *Phys. Status Solidi B* **195**, 425 (1996).
- [11] H.-H. Lin, L. Balents, and M. P. Fisher, *Phys. Rev. B* **56**, 6569 (1997).
- [12] N. Bulut, D. J. Scalapino, and R. T. Scalettar, *Phys. Rev. B* **45**, 5577 (1992).
- [13] K. Kuroki, T. Kimura, and R. Arita, *Phys. Rev. B* **66**, 184508 (2002).
- [14] T. A. Maier and D. J. Scalapino, *Phys. Rev. B* **84**, 180513(R) (2011).
- [15] V. Mishra, D. J. Scalapino, and T. A. Maier, *Sci. Rep.* **6**, 32078 (2016).
- [16] M. Nakata, D. Ogura, H. Usui, and K. Kuroki, *Phys. Rev. B* **95**, 214509 (2017).
- [17] T. A. Maier, V. Mishra, G. Balduzzi, and D. J. Scalapino, *Phys. Rev. B* **99**, 140504(R) (2019).
- [18] S. Karakuzu, S. Johnston, and T. A. Maier, *Phys. Rev. B* **104**, 245109 (2021).
- [19] K. Matsumoto, D. Ogura, and K. Kuroki, *J. Phys. Soc. Jpn.* **89**, 044709 (2020).
- [20] D. Kato and K. Kuroki, *Phys. Rev. Res.* **2**, 023156 (2020).
- [21] H. Sun, M. Huo, X. Hu, J. Li, Z. Liu, Y. Han, L. Tang, Z. Mao, P. Yang, B. Wang, J. Cheng, D.-X. Yao, G.-M. Zhang, and M. Wang, *Nature* (2023).
- [22] Z. Liu, M. Huo, J. Li, Q. Li, Y. Liu, Y. Dai, X. Zhou, J. Hao, Y. Lu, M. Wang, and H.-H. Wen, (2023), arXiv:2307.02950.
- [23] J. Hou, P. T. Yang, Z. Y. Liu, J. Y. Li, P. F. Shan, L. Ma, G. Wang, N. N. Wang, H. Z. Guo, J. P. Sun, Y. Uwatoko, M. Wang, G. M. Zhang, B. S. Wang, and J. G. Cheng, (2023), arXiv:2307.09865.
- [24] Y. Zhang, D. Su, Y. Huang, H. Sun, M. Huo, Z. Shan, K. Ye, Z. Yang, R. Li, M. Smidman, M. Wang, L. Jiao, and H. Yuan, (2023), arXiv:2307.14819.
- [25] Y. Shen, M. Qin, and G.-M. Zhang, (2023), arXiv:2306.07837.
- [26] Q.-G. Yang, D. Wang, and Q.-H. Wang, (2023), arXiv:2306.03706.
- [27] V. Christiansson, F. Petocchi, and P. Werner, (2023), arXiv:2306.07931.
- [28] W. Wu, Z. Luo, D.-X. Yao, and M. Wang, (2023), arXiv:2307.05662.
- [29] Z. Liao, L. Chen, G. Duan, Y. Wang, C. Liu, R. Yu, and Q. Si, (2023), arXiv:2307.16697.
- [30] X.-Z. Qu, D.-W. Qu, J. Chen, C. Wu, F. Yang, W. Li, and G. Su, (2023), arXiv:2307.16873.
- [31] H. Oh and Y.-H. Zhang, (2023), arXiv:2307.15706.
- [32] Z. Luo, X. Hu, M. Wang, W. Wu, and D.-X. Yao, (2023), arXiv:2305.15564.
- [33] Y.-B. Liu, J.-W. Mei, F. Ye, W.-Q. Chen, and F. Yang, (2023), arXiv:2307.10144.
- [34] Y. Cao and Y. feng Yang, (2023), arXiv:2307.06806.
- [35] C. Lu, Z. Pan, F. Yang, and C. Wu, (2023), arXiv:2307.14965.
- [36] X. Chen, P. Jiang, J. Li, Z. Zhong, and Y. Lu, (2023), arXiv:2307.07154.
- [37] Y. Zhang, L.-F. Lin, A. Moreo, and E. Dagotto, (2023), arXiv:2306.03231.
- [38] Y. Zhang, L.-F. Lin, A. Moreo, T. A. Maier, and E. Dagotto, (2023), arXiv:2307.15276.
- [39] F. Lechermann, J. Gondolf, S. Botzel, and I. M. Eremin, (2023), arXiv:2306.05121.
- [40] Y. Yang, G.-M. Zhang, and F.-C. Zhang, (2023), arXiv:2308.01176.
- [41] K. Jiang, Z. Wang, and F.-C. Zhang, (2023), arXiv:2308.06771.
- [42] Y. Gu, C. Le, Z. Yang, X. Wu, and J. Hu, (2023), arXiv:2306.07275.
- [43] Z. Pan, C. Lu, F. Yang, and C. Wu, (2023), arXiv:2309.06173.
- [44] J.-X. Zhang, H.-K. Zhang, Y.-Z. You, and Z.-Y. Weng, (2023), arXiv:2309.05726.
- [45] Z. Luo, B. Lv, M. Wang, W. Wu, and D. xin Yao, (2023), arXiv:2308.16564.
- [46] R. Jiang, J. Hou, Z. Fan, Z.-J. Lang, and W. Ku, (2023), arXiv:2308.11614.
- [47] D.-C. Lu, M. Li, Z.-Y. Zeng, W. Hou, J. Wang, F. Yang, and Y.-Z. You, (2023), arXiv:2308.11195.
- [48] Y.-H. Tian, Y. Chen, J.-M. Wang, R.-Q. He, and Z.-Y. Lu, (2023), arXiv:2308.09698.
- [49] Q. Qin and Y. feng Yang, (2023), arXiv:2308.09044.
- [50] J. Huang, Z. D. Wang, and T. Zhou, (2023), arXiv:2308.07651.
- [51] Y. Zhang, L.-F. Lin, A. Moreo, T. A. Maier, and E. Dagotto, (2023), arXiv:2308.07386.
- [52] H. Sakakibara, N. Kitamine, M. Ochi, and K. Kuroki, (2023), arXiv:2306.06039.
- [53] J. P. Perdew, A. Ruzsinszky, G. I. Csonka, O. A. Vydrov, G. E. Scuseria, L. A. Constantin, X. Zhou, and K. Burke, *Phys. Rev. Lett.* **100**, 136406 (2008).
- [54] G. Kresse and D. Joubert, *Phys. Rev. B* **59**, 1758 (1999).
- [55] G. Kresse and J. Hafner, *Phys. Rev. B* **47**, 558 (1993).
- [56] G. Kresse and J. Hafner, *Phys. Rev. B* **49**, 14251 (1994).
- [57] G. Kresse and J. Furthmüller, *Comput. Mater. Sci.* **6**, 15 (1996).
- [58] G. Kresse and J. Furthmüller, *Phys. Rev. B* **54**, 11169 (1996).
- [59] A. Togo and I. Tanaka, *Scr. Mater.* **108**, 1 (2015).
- [60] N. Marzari and D. Vanderbilt, *Phys. Rev. B* **56**, 12847 (1997).
- [61] I. Souza, N. Marzari, and D. Vanderbilt, *Phys. Rev. B* **65**, 035109 (2001).
- [62] G. Pizzi *et al.*, *J. Phys.: Cond. Matter* **32**, 165902 (2020).
- [63] N. E. Bickers, D. J. Scalapino, and S. R. White, *Phys. Rev. Lett.* **62**, 961 (1989).
- [64] N. E. Bickers and S. R. White, *Phys. Rev. B* **43**, 8044 (1991).
- [65] A. I. Lichtenstein and M. I. Katsnelson, *Phys. Rev. B* **57**, 6884 (1998).
- [66] K. Yada and H. Kontani, *J. Phys. Soc. Jpn.* **74**, 2161 (2005).
- [67] M. Mochizuki, Y. Yanase, and M. Ogata, *Phys. Rev. Lett.* **94**, 147005 (2005).
- [68] H. Ikeda, R. Arita, and J. Kuneš, *Phys. Rev. B* **81**, 054502 (2010).
- [69] K. Momma and F. Izumi, *J. Appl. Crystallogr.* **44**, 1272 (2011).
- [70] H. Sakurai *et al.*, in preparation (2023).
- [71] R. Matsumoto, Y. Sasama, M. Fujioka, T. Irifune, M. Tanaka, T. Yamaguchi, H. Takeya, and Y. Takano, *Rev. Sci. Instrum.* **87**, 076103 (2016).
- [72] R. Matsumoto, A. Yamashita, H. Hara, T. Irifune, S. Adachi, H. Takeya, and Y. Takano, *Applied Physics Express* **11**, 053101 (2018).

- [73] G. J. Piermarini, S. Block, J. D. Barnett, and R. A. Forman, *J. Appl. Phys.* **46**, 2774 (1975).
- [74] Y. Akahama and H. Kawamura, *J. Appl. Phys.* **96**, 3748 (2004).
- [75] R. Matsumoto, Z. Hou, M. Nagao, S. Adachi, H. Hara, H. Tanaka, K. Nakamura, R. Murakami, S. Yamamoto, H. Takeya, T. Irifune, K. Terakura, and Y. Takano, *Science and Technology of Advanced Materials* **19**, 909 (2018).
- [76] R. Matsumoto, T. Irifune, M. Tanaka, H. Takeya, and Y. Takano, *Japanese Journal of Applied Physics* **56**, 05FC01 (2017).
- [77] Z. Zhang and M. Greenblatt, *J. Solid State Chem.* **117**, 236 (1995).
- [78] J. Zhang, H. Zheng, Y.-S. Chen, Y. Ren, M. Yonemura, A. Huq, and J. F. Mitchell, *Phys. Rev. Mater.* **4**, 083402 (2020).
- [79] V. Voronin, I. Berger, V. Cherepanov, L. Gavrilova, A. Petrov, A. Ancharov, B. Tolochko, and S. Nikitenko, *Nuclear Instruments and Methods in Physics Research Section A: Accelerators, Spectrometers, Detectors and Associated Equipment* **470**, 202 (2001), proceedings of the 13th National Synchrotron Radiation Conference.
- [80] C. D. Ling, D. N. Argyriou, G. Wu, and J. Neumeier, *J. Solid State Chem.* **152**, 517 (2000).
- [81] M. U. Nagell, S. Kumar, M. H. Sørby, H. Fjellvåg, and A. O. Sjøstad, *Phase Transitions* **88**, 979 (2015).
- [82] S. Kumar, Ø. Fjellvåg, A. O. Sjøstad, and H. Fjellvåg, *J. Magn. Magn. Mater.* **496**, 165915 (2020).
- [83] M. Periyasamy, L. Patra, Ø. S. Fjellvåg, P. Ravindran, M. H. Sørby, S. Kumar, A. O. Sjøstad, and H. Fjellvåg, *ACS Appl. Electron. Mater.* **3**, 2671 (2021).
- [84] A. Olafsen, H. Fjellvåg, and B. C. Hauback, *J. Solid State Chem.* **151**, 46 (2000).
- [85] B.-Z. Li, C. Wang, P. T. Yang, J. P. Sun, Y.-B. Liu, J. Wu, Z. Ren, J.-G. Cheng, G.-M. Zhang, and G.-H. Cao, *Phys. Rev. B* **101**, 195142 (2020).
- [86] S. Huangfu, X. Zhang, and A. Schilling, *Phys. Rev. Res.* **2**, 033247 (2020).
- [87] S. Huangfu, G. D. Jakob, X. Zhang, O. Blacque, P. Pupal, E. Pomjakushina, F. O. von Rohr, and A. Schilling, *Phys. Rev. B* **101**, 104104 (2020).
- [88] H. Li, X. Zhou, T. Nummy, J. Zhang, V. Pardo, W. E. Pickett, J. F. Mitchell, and D. S. Dessau, *Nat. Commun.* **8**, 704 (2017).
- [89] D. Puggioni and J. M. Rondinelli, *Phys. Rev. B* **97**, 115116 (2018).
- [90] H. Sakakibara, H. Usui, K. Kuroki, R. Arita, and H. Aoki, *Phys. Rev. Lett.* **105**, 057003 (2010).
- [91] H. Sakakibara, H. Usui, K. Kuroki, R. Arita, and H. Aoki, *Phys. Rev. B* **85**, 064501 (2012).
- [92] H. Sakakibara, K. Suzuki, H. Usui, S. Miyao, I. Maruyama, K. Kusakabe, R. Arita, H. Aoki, and K. Kuroki, *Phys. Rev. B* **89**, 224505 (2014).
- [93] For a brief summary on the effect of incipient bands in spin-fluctuation-mediated superconductivity, see N. Kitamine, M. Ochi, and K. Kuroki, arXiv:2308.12750.
- [94] M. Zhang, C. Pei, Q. Wang, Y. Zhao, C. Li, W. Cao, S. Zhu, J. Wu, and Y. Qi, (2023), arXiv:2309.01651.